

Casimir effect with dielectric matter in salted water and implications at the cell scale

Larissa Inácio 

Centre of Excellence ENSEMBLE3, Sp. z o. o.,
Wolczynska Str. 133, 01-919, Warsaw, Poland

Felipe S. S. Rosa  and Paulo A. Maia Neto *

Instituto de Física, Universidade Federal do Rio de Janeiro,
21941-972 Rio de Janeiro, Rio de Janeiro, Brazil

Astrid Lambrecht 

Forschungszentrum Jülich, 52425 Jülich, Germany and
RWTH Aachen University, 52062 Aachen, Germany

Serge Reynaud †

Laboratoire Kastler Brossel, Sorbonne Université, CNRS,
ENS-PSL, Collège de France, 75252 Paris, France

(Dated: January 15, 2026)

The Casimir interaction in salted water contains a universal contribution of electromagnetic fluctuations that makes it of a longer range than previously thought. The universal contribution dominates non universal ones at the distances relevant for actin fibers inside the cell. We discuss universal and non-universal contributions with a model mimicking biological matter. We also show that the universal Casimir effect should have important implications at the cell scale.

I. INTRODUCTION

Quantum physics was born when Planck wrote the first quantum law where he explained the properties of black body radiation [1]. This law gave the mean energy per mode of the electromagnetic field as the product of the energy of a photon $\hbar\omega$ by a mean number \bar{n}_ω of thermal photons per mode at frequency ω . Approximately ten years later, Planck [2] added an extra term $\frac{1}{2}\hbar\omega$ to the mean energy per mode. This marked the appearance in physics of the zero-point fluctuations which have superseded the now abandoned reasoning of the paper in which they were introduced [3, 4].

While the original Planck's law fell off the expectation $k_B T$ by a constant offset $(-\frac{\hbar\omega}{2})$ at high temperatures ($T \rightarrow \infty$), the second law including zero-point fluctuations had the correct classical limit [5]. The modern writing of the mean energy per mode makes this property obvious since all terms in the high-temperature expansion go to 0 at $T \rightarrow \infty$ but the dominant one

$$\left(\frac{1}{2} + \bar{n}_\omega\right)\hbar\omega = \frac{\hbar\omega}{2} \coth \frac{\hbar\omega}{2k_B T} \quad \xrightarrow{T \rightarrow \infty} k_B T + O\left(\frac{1}{T}\right). \quad (1)$$

Discussions on zero-point fluctuations were active before their precise nature was better understood as the full development of quantum theory took place [6]. Vacuum fluctuations, the zero-point fluctuations of electromagnetic fields in empty space, were introduced in old quantum theory [7, 8].

Nowadays, zero-point fluctuations are considered as a consequence of the non-commutative character of quantum observables [9–12] (these papers are reproduced and commented on [13], where English translations are given for papers written in German). The dispersions of these fluctuations are specified by inequalities deduced from the commutators of observables [14] (history discussed, for example, in [15–17]). Vacuum fluctuations are now defined by the quantum theory of electromagnetic field [18], with each field mode represented by canonical variables analogous to those of an harmonic oscillator. This theory leads to a full quantum derivation of Einstein's description of absorption, stimulated and spontaneous emission processes [19]. Vacuum fluctuations have many important effects in atomic and subatomic physics, such as the Lamb shift and radiative corrections [20–24].

* pamn@if.ufrj.br

† serge.reynaud@lkb.upmc.fr

In this paper, we focus the discussions on the mechanical effects due to the radiation pressure of these fluctuations that are Casimir forces [25], and related Casimir-Polder and van der Waals forces [26–28]. In his initial work, Casimir studied an idealized problem with two perfectly reflecting plane mirrors in electromagnetic vacuum at zero temperature. Since then, a large number of papers has generalized the description to make it more realistic in terms of material properties and geometry (a review with many references can be found in [29]). Meanwhile, more and more sophisticated experiments have, in particular, measured precisely the forces between metallic reflecting surfaces in empty space (reviews and references in [30–35]).

We stress at this point that most experiments are performed at room temperature, so that thermal and zero-point fluctuations have to be considered together. The study of Casimir effect in the presence of thermal fluctuations has a long history [36–38]. It is conveniently treated by using the Matsubara summation technique [39]. The latter is directly related to formula (1) as Matsubara frequencies are nothing but the poles of the hyperbolic cotangent function, namely [40]

$$\frac{1}{2} \coth \frac{\hbar\omega}{2k_B T} = \sum_{n=-\infty}^{+\infty} \frac{k_B T}{\hbar(\omega - i\xi_n)} , \quad \xi_n = n \frac{2\pi k_B T}{\hbar} . \quad (2)$$

An advantage of the Matsubara technique is that the high-temperature limit of the interaction is given by the term at zero frequency, that is, the pole at $\omega = 0$ in formulas (1-2). This contribution has a universal character [41, 42] since it does not depend on details of the variation with frequency of the electromagnetic response functions (details discussed below).

For the most common experimental configuration using metallic scatterers in empty space ([42] and references therein), this universal limit can only be met at distances larger than the thermal wavelength in vacuum, where the force is very small and difficult to measure with precision (see the experiments discussed in [43, 44]). There exists, however, another configuration of great interest in this respect, which involves dielectric matter in electrolytes. In this case, the Casimir force can be both large and dominated by the universal term at not too large distances. This configuration has been studied in previous theoretical and experimental papers [45–49] and will be reviewed in the following.

This universal Casimir effect in electrolytes is of particular relevance at the interface of physics and biology, as it may have a large impact on the mechanics of biological systems at the cell scale, a point that has been recently emphasized [50] and will also be revisited below.

II. SCATTERING THEORY OF CASIMIR INTERACTION IN ELECTROLYTES

We first describe in this section the scattering theory of the Casimir effect in electrolytes in the simplest geometry of two bulks of matter with parallel plane interfaces, separated by an electrolyte layer [46], see Fig. 1.

As we consider the Casimir interaction between objects immersed in an electrolyte, the key “novelty” is that the dissolved ions give rise to important nonlocal effects. Such nonlocality, also referred to as spatial dispersion, manifests itself in a k -dependence of the permittivity in reciprocal space and also in the emergence of a nontrivial tensorial character of the electrolyte permittivity

$$\epsilon(\omega) \longrightarrow \epsilon_{ij}(\omega, \mathbf{k}) \quad (3)$$

The main consequence of the nonlocality of the medium is the support of longitudinal modes, besides the usual transverse electromagnetic fluctuations. The medium allows for 3 independent polarizations: transverse electric (TE), transverse magnetic (TM) and longitudinal (ℓ), and the extra degree of freedom for the fluctuations has quite important consequences for dispersion interactions [46].

The most economical way of writing the Casimir energy is by reinterpreting it as a reverberation problem for the electromagnetic fluctuations, and then making a Wick rotation to imaginary frequencies [40]. In order to keep things as simple as possible, we assume that the bulk materials are strictly (spatially) local. The Wick rotation produces a Matsubara sum over the frequencies defined in (2)

$$\mathcal{F}_{\text{Cas}} = \mathcal{F}_0 + \sum_{n=1}^{\infty} \mathcal{F}_n . \quad (4)$$

In the total Casimir free energy \mathcal{F}_{Cas} , we have separated the term \mathcal{F}_0 , corresponding to the zero Matsubara frequency, as it plays the main role in the discussions of this paper. The other terms \mathcal{F}_n , each corresponding to a nonzero frequency ξ_n , are discussed for the two-bulks geometry in [46], and they will be discussed for the two-slabs geometry in §V below.

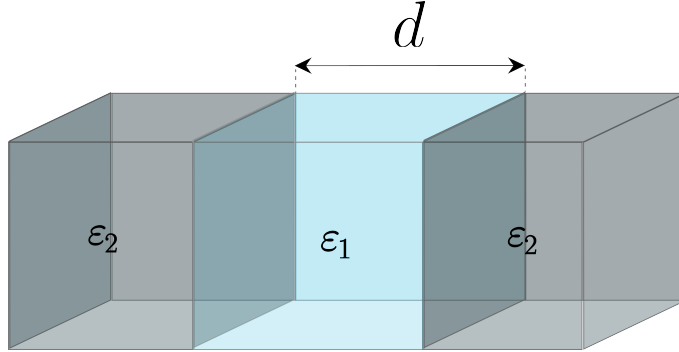


FIG. 1. Sketch view of the two-bulks configuration, with d the distance between the two parallel interfaces, ε_1 and ε_2 the dielectric functions for water and immersed matter.

It can be shown [46] that the TM and ℓ fluctuations are coupled at the interfaces between the bulks and medium, but, fortunate as it may seem, it turns out that the TE term vanishes in the limit $\xi \rightarrow 0$ and the TM- ℓ contributions actually uncouple from each other [51], thus yielding for an area A

$$\mathcal{F}_0 = \underbrace{A \frac{k_B T}{2} \int \frac{d^2 k}{(2\pi)^2} \ln(1 - e^{-2kd})}_{-A \frac{k_B T}{16\pi} \frac{\zeta(3)}{d^2}} + \underbrace{A \frac{k_B T}{2} \int \frac{d^2 k}{(2\pi)^2} \ln(1 - r_\ell^2 e^{-2\sqrt{k^2 + \lambda_D^{-2}}d})}_{\mathcal{F}_0^{(\ell)}}. \quad (5)$$

We rewrite this expression by highlighting the first (TM) term that will henceforth be referred to as the *universal* Casimir contribution $\mathcal{F}_{\text{univ}}^{\text{bulk}}$ as it depends only on the temperature and geometry

$$\mathcal{F}_0 = \mathcal{F}_{\text{univ}}^{\text{bulk}} + \mathcal{F}_0^{(\ell)} \quad , \quad \mathcal{F}_{\text{univ}}^{\text{bulk}} = -\frac{A}{12\pi d^2} \frac{H}{k_B T} \quad , \quad H = \frac{3\zeta(3)}{4} k_B T. \quad (6)$$

The Hamaker constant H depends only on temperature ($H \simeq 0.9 k_B T$ with ζ denoting the Riemann function and $\zeta(3) \simeq 1.202$ the Apery's constant), and it gives \mathcal{F} through a multiplication by a dimensionless geometrical quantity. As $\mathcal{F}_{\text{univ}}^{\text{bulk}}$ is proportional to temperature, the associated entropy is simply deduced to be such that the mechanical energy $\mathcal{F}_{\text{univ}}^{\text{bulk}} + T\mathcal{S}_{\text{univ}}^{\text{bulk}}$ vanishes, which means that the universal Casimir interaction is a purely entropic effect. These properties are still true for the other geometries considered below, with different expressions, naturally.

The second term in (5) is the longitudinal contribution at zero Matsubara frequency, and it is determined by the reflection amplitude r_ℓ and the Debye length λ_D

$$r_\ell = \frac{\epsilon_b(0)\sqrt{k^2 + \lambda_D^{-2}} - \epsilon_2(0)k}{\epsilon_b(0)\sqrt{k^2 + \lambda_D^{-2}} + \epsilon_2(0)k} \quad , \quad \lambda_D = \sqrt{\frac{\epsilon_b(0)k_B T}{n^2 m}}, \quad (7)$$

where n is the ionic concentration in the electrolyte, m is the ion mass, and ϵ_b is the dielectric permittivity of pure water (i.e., the permittivity of water without the ionic contribution).

In the long distance limit, the longitudinal part $\mathcal{F}_0^{(\ell)}$ is exponentially suppressed by the Debye screening with typical length λ_D

$$\mathcal{F}_0^{(\ell)} \propto e^{-2d/\lambda_D}. \quad (8)$$

This is the first major takeaway of this paper: there is indeed a screening of the contribution $\mathcal{F}_0^{(\ell)}$ of longitudinal modes across the electrolyte, but the universal contribution $\mathcal{F}_{\text{univ}}^{\text{bulk}}$ is *unscreened* as it arises from the transverse electromagnetic fluctuations. This property was first demonstrated in the framework of a macroscopic description of the dielectric response of salted water [46] and it has been confirmed since then by the molecular dynamics simulations presented in [50]. This has far-reaching consequences for physical and even biological systems, which we will discuss in the following.

An important remark has to be made clear at this point. The discussions just presented on transverse and longitudinal fluctuations treat fields in the vicinity of zero frequency rather than at zero frequency. In technical terms, what has been calculated is given by a residue associated with the pole at $\omega = 0$ of the cotangent function in (2). The physical origin of the effect is simply the divergence as $\frac{k_B T}{\hbar\omega}$ of the number of photons in a field mode with frequency close to $\omega = 0$, leaving in the end a finite contribution to the free energy.

III. EXPERIMENTAL EVIDENCE WITH OPTICAL TWEEZERS

Optical tweezers [52] are an ideal tool to measure interaction forces in aqueous media, and several applications in biology have been developed [53, 54] over the years. Since the trap stiffness is proportional to the beam laser power, the system can be tuned to match the required order of magnitude. Standard single-beam traps are most effective for particles whose refractive indexes are slightly higher than that of the surrounding medium. Conveniently, this is also the condition that minimizes the non-universal contributions $\mathcal{F}_{n \geq 1}$ which depend on the reflection (or more generally scattering) amplitudes at the interface between the material and the host medium.

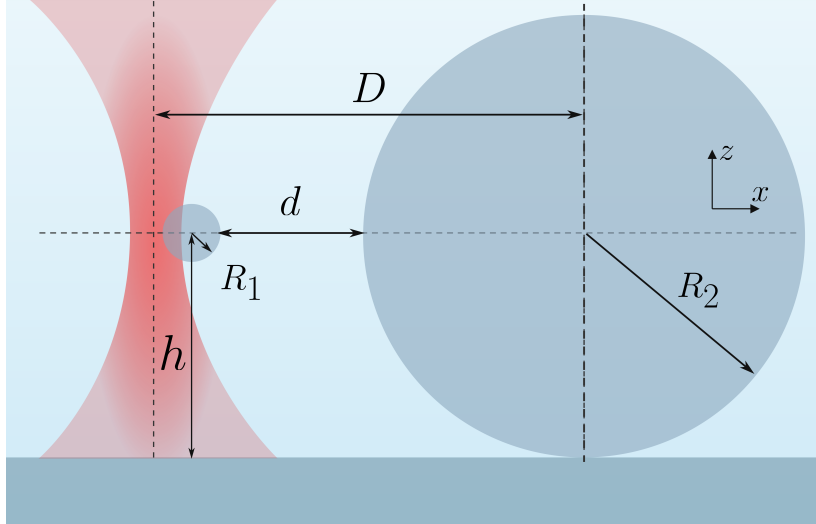


FIG. 2. Principle of the experiment reported in Ref. [47]: a silica microsphere (radius R_1) is held by a tightly focused laser beam close to a larger silica microsphere (radius R_2) which is attached to the glass slide at the bottom of the sample chamber. The distance D between the larger microsphere and the laser axis is controlled by using a piezoelectric nano-positioning system. The Brownian fluctuations of the trapped microsphere are measured for different values of D . The distance of closest approach of the two spheres is denoted d and the height of the small sphere above the glass slide h .

The universal Casimir interaction between two silica microspheres immersed in salted water has been measured with optical tweezers [47]. The experimental scheme is sketched in Fig. 2. Brownian fluctuations of a small silica microsphere (radius $R_1 = 2.4 \mu\text{m}$) held by optical tweezers were measured along the x and y directions transverse to the laser beam. The interaction energy was then observed through the modification of the fluctuations along the x -axis connecting the sphere centers, as the larger microsphere (radius $R_2 = 12 \mu\text{m}$), adhered to the glass slide at the bottom of the sample, was approached by employing a piezoelectric nano-positioning system. The sample was also displaced vertically to align the sphere centers so as to have $h = R_2$, where h is the height of the small microsphere with respect to the glass slide. While fluctuations along x captured the interaction signal, fluctuations along y were not modified, showing the absence of optical binding or of any other perturbation of the optical force in this configuration with near index matching. Since the trapping beam was circularly polarized, the Brownian fluctuations along y accumulated over several experimental runs were employed to infer the optical potential relevant for the interaction direction x . As an additional check, the resulting optical potential was shown to agree with the Mie-Debye theory of optical tweezers [55, 56] as well as with standard Stokes calibration [57], with the latter implemented in the absence of the larger microsphere.

The interaction energy for distances above 100 nm was then obtained by subtracting the optical potential from the total energy as determined by the Brownian dynamics along the x -direction. For moderate salt concentrations, the interaction was dominated by the electrostatic double layer interaction. In order to suppress such interaction, a second experiment reported in Ref. [47] employed a high salt concentration (strong screening with $\lambda_D = 0.65 \text{ nm}$). In this second case, the interaction was completely dominated by the universal Casimir contribution discussed in the previous section.

Figure 3 shows the resulting Casimir energy in units of $k_B T$ versus distance d of closest approach (see Fig. 2). The red curve represents the non-universal contribution accounting for the positive Matsubara frequencies $\xi_{n \geq 1}$. The calculation is based on Mie scattering by dielectric spheres in water [58]. The red curve thus represents the generalization for the geometry of two spheres of the standard theoretical prediction for the Casimir interaction in salted water [59], which is usually considered within the parallel planar interfaces setup or within the corresponding

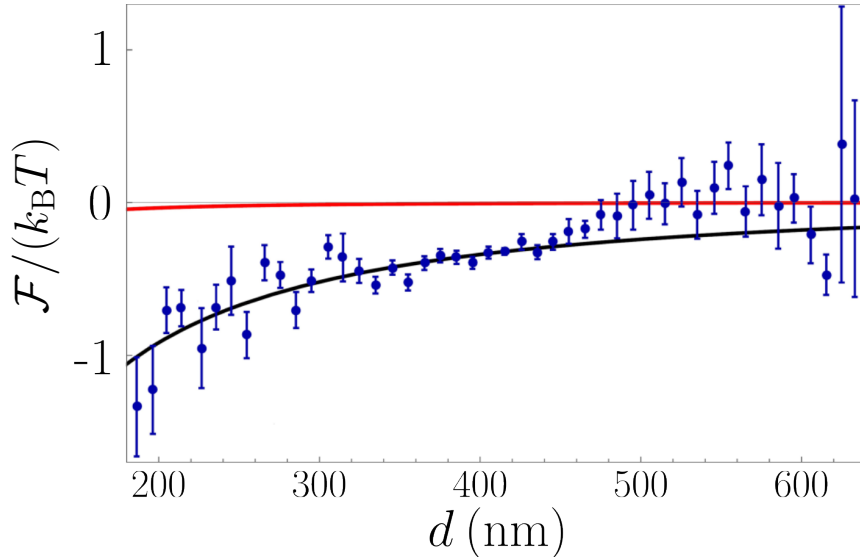


FIG. 3. Variation of the Casimir interaction energy (in units of the thermal energy $k_B T$) with the distance d between two dielectric microspheres in salted water for the setup depicted in Fig. 2. Experimental points are shown with their error bars (blue). The old approach relying on overlooking the universal contribution (red) leads to much too small values to be compatible with the experimental data. New theory (black), with the universal contribution included, agrees fairly well with experiments (with no fitting). Adapted from Pires et al. [47] under the terms of the Creative Commons Attribution 4.0 International license.

proximity force approximation. The longitudinal contribution $\mathcal{F}_0^{(\ell)}$ is not included as it is negligible at both moderate and high salt concentrations employed in Ref. [47], due to the fact that the distances are much larger than the corresponding Debye screening lengths. Indeed, $\mathcal{F}_0^{(\ell)}$ is given by the second term in the right-hand-side of Eq. (5) for parallel planar interfaces and calculated for two spheres in Ref. [60]. In both cases, $\mathcal{F}_0^{(\ell)}$ becomes exponentially small at distances larger than λ_D .

The black curve in Fig. 3 stands for the total Casimir interaction, including the universal contribution arising from TM modes in the zero frequency limit. Like the non-universal contribution, it is calculated exactly for the geometry of two dielectric spheres in salted water as described in Refs. [48, 49] (see also Sec. IV below). The comparison between the black and red curves indicates that the universal contribution dominates the Casimir interaction for distances above 200 nm. More importantly, the unscreened, universal Casimir contribution provides an excellent description of the data, with no fitting parameter, in contrast with the standard approach that overlooks the contribution of TM modes and is excluded by the experimental data shown in Fig. 3.

IV. UNIVERSAL CASIMIR INTERACTION IN THE TWO-SPHERES OR TWO-CYLINDERS GEOMETRIES

The universal Casimir interaction that is the high-temperature limit of the expression in the case of very efficient Debye screening has been calculated in the two-spheres [48, 49] and two-cylinders [50] geometries. As in the two-bulks geometry considered previously, it arises from the term $n = 0$ in the Matsubara sum appearing due to transverse electromagnetic fluctuations, and it does not depend on details of the frequency dependence of dielectric functions.

The associated free energy is the product of the thermal energy scale $k_B T$ by a dimensionless function f which now depends in a non trivial manner on the geometrical parameters. In the two-spheres geometry, we have

$$\mathcal{F}_{\text{univ}}^{\text{sph}} = -k_B T f(d, R_1, R_2) . \quad (9)$$

The Casimir interaction is captured in the function f which has been calculated for two dielectric spheres in salted water [48, 49]. It does not depend on temperature (the effect is purely entropic) and it is a dimensionless function of the two ratios which can be formed with the three length parameters d (note that it was denoted L in [48, 49]), R_1 and R_2 (radii of the two spheres; see Fig. 4a).

The function f is calculated within the scattering theory of the Casimir effect [40]. It is a sum over all field modes of scattering operators involving an arbitrary number of round-trips in the cavity formed by the two objects. In

the so-called dipolar limit where the spheres have small sizes in comparison with the distance, the contributions of large numbers of round-trips are negligible. In this small size approximation (SSA) or equivalently long distance approximation, f is proportional to the two volumes R_1^3 and R_2^3 , and inversely proportional to the sixth power of distance [48, 49]

$$f_{\text{SSA}} = \frac{3R_1^3 R_2^3}{4d^6} . \quad (10)$$

In the opposite limit of a short distance between the spheres, the exact result involves large numbers of round-trips, and it tends to an expression related to the two-bulks geometry through the proximity force approximation [61]. In this PFA limit, f is proportional to the effective radius R_{eff} defined from the two radii R_1 and R_2 , and inversely proportional to the distance

$$f_{\text{PFA}} = \zeta(3) \frac{R_{\text{eff}}}{8d} , \quad R_{\text{eff}} = \frac{R_1 R_2}{R_1 + R_2} . \quad (11)$$

The function f has a universal expression which does not depend on the details of the variation with frequency of the permittivity functions of either the dielectric matter in the spheres or of salted water constituting the immersion medium. The result is conveniently conveyed - just like in Fig. 1(b) of [48] - as a function $f_u(x)$ of two dimensionless parameters

$$x = \frac{d}{R_{\text{eff}}} , \quad u = \frac{R_1 R_2}{(R_1 + R_2)^2} , \quad (12)$$

where x is an aspect ratio for the distance d , and u an aspect ratio for the radii. The fact that f depends only on x and u is a remarkable scale-invariance property meaning that f is unchanged when the three geometrical dimensions d, R_1, R_2 are multiplied by a common factor.

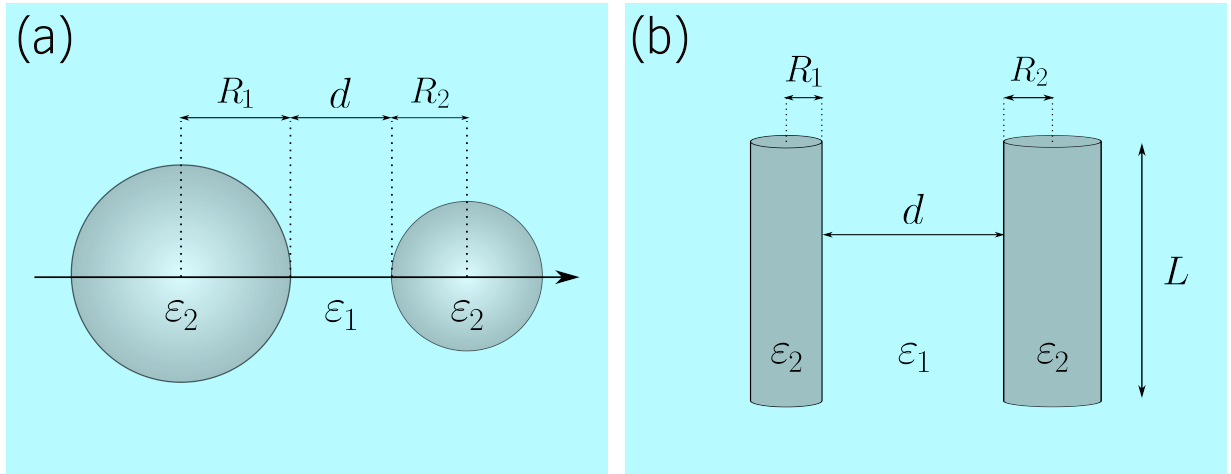


FIG. 4. Geometry for two spheres (a) or two cylinders (b) immersed in salted water. R_1 and R_2 are the radii of spheres or cylinders, and d the distance of closest approach (ε_1 and ε_2 defined as for Fig.1).

A more subtle property appears when f is written (see Fig. 2 in [48]) in terms of another parameter

$$y = \frac{(d + R_1 + R_2)^2 + R_1^2 + R_2^2}{2R_1 R_2} = 1 + x \left(1 + \frac{ux}{2} \right) . \quad (13)$$

The value of f thus appears to depend mainly on y , which reveals an approximate conformal invariance of geometrical dependence of the free energy [48, 49]. This property has been used in [49] to give a simple formula which can be applied to a wide range of geometrical parameters. This formula is sufficient for the salinity of biological media and at ambient temperature. The obtained free energy $\mathcal{F}_{\text{univ}}^{\text{sph}}$ is larger than $k_B T$ ($f \geq 1$) only for spheres very close to each other, that is the geometry in which the universal Casimir interaction has been experimentally measured (see §III).

In order to compare the two-spheres case and the two-cylinders one discussed below, we consider the geometry of two spheres with equal radii $R_1 = R_2 = R$ and draw in Fig. 5a the corresponding function f versus the geometric

parameter x defined in (12). The grayed out band in the figure shows where $f < 1$, which is also where the binding energy $|\mathcal{F}|$ is smaller than the Brownian motion energy scale. The figure shows that the universal Casimir effect dominates the Brownian energy $k_B T$ for distances $d < 0.09 R_{\text{eff}}$. Note that, for the geometry with different radii employed in the optical tweezers experiment of §III, , the order of magnitude for this border $|\mathcal{F}_{\text{univ}}^{\text{sph}}| \simeq k_B T$ is at $d \approx 0.2 \mu\text{m}$, which is indeed the scale of distances probed in Ref. [47].

We now come to the discussion of the configuration with two dielectric cylinders in salted water. This configuration makes the interaction larger than in the two-spheres case as it scales as the length L of the cylinders. The geometry is shown in Fig. 4b with two cylinders with radii R_1, R_2 at a distance d of closest approach. In this geometry, the universal Casimir free energy is the product of the thermal energy $k_B T$ by two dimensionless factors $\frac{L}{d}$ and ϕ

$$\mathcal{F}_{\text{univ}}^{\text{cyl}} = -k_B T \frac{L}{d} \phi(d, R_1, R_2) . \quad (14)$$

The physics of the universal interaction is captured in the function ϕ which has been calculated in [50]. The remarks written after equation (9) remain valid here as ϕ does not depend on temperature and is a dimensionless function of two ratios of the three geometrical quantities d, R_1 and R_2 .

In order to discuss the implications of these results for biological systems in section VI, we depict in Fig. 5b the function ϕ for two cylinders with equal radii $R_1 = R_2 = R$. The function ϕ is plotted versus the geometric parameter x defined as in (12), but for cylinders. The grayed out band in the figure shows where $\phi < 0.001$, that is where the binding energy $|\mathcal{F}|$ is smaller than the Brownian motion energy scale for $L = 1000 d$ (see the discussions to be presented in section VI). The take-home message from the figure is that the universal Casimir free energy dominates the Brownian motion energy $k_B T$ imposed by the surrounding water over a broad range of parameters, including in particular distances d of the order of R_{eff} . The striking difference between the two-spheres case (Fig. 5a) and the two-cylinders one (Fig. 5b) is simply due to the presence of the large factor $\frac{L}{d}$ in formula (14) which makes $|\mathcal{F}_{\text{univ}}^{\text{cyl}}|$ larger than $k_B T$ in a wider range of parameters.

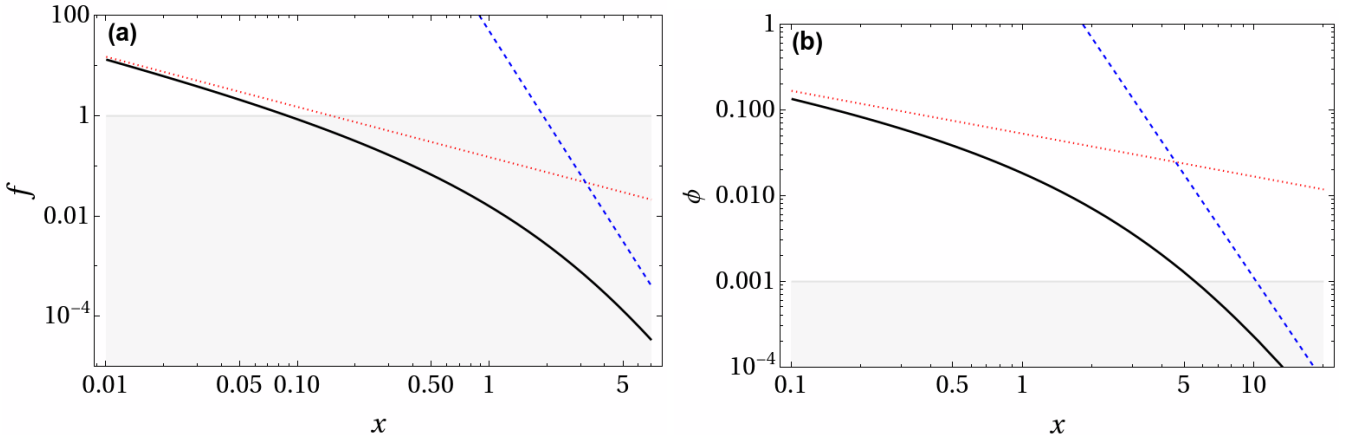


FIG. 5. Universal functions (solid black curves) showing the variations of the universal free energy versus $x = d/R_{\text{eff}}$: (a) function f calculated for two spheres with equal radii; (b) function ϕ calculated for two cylinders with equal radii. In both plots, red dotted and blue dashed lines represent the proximity force and small size approximations giving the asymptotic behaviors at $x \ll 1$ and $x \gg 1$ respectively.

Both functions in Fig. 5 agree with the proximity force approximation (red dotted curve) at short separations and with the small size approximation (blue dashed line) at long distances. For completeness, we give the PFA and SSA expressions for the case of two cylinders

$$\phi_{\text{PFA}} = \frac{\zeta(3)}{32} \sqrt{\frac{2R_{\text{eff}}}{d}} , \quad \phi_{\text{SSA}} = \frac{891\pi}{4096} \frac{R_1^2 R_2^2}{d^4} . \quad (15)$$

These expressions have to be compared to eqs. (11) and (10) respectively. In particular the changes of power laws have clear meanings. For the PFA, ϕ is proportional to $\sqrt{R_{\text{eff}}/d}$ because there is only one curvature radius in a direction orthogonal to the distance for cylinders (there are two of them for spheres and f is proportional to R_{eff}/d). For the SSA, the extensive quantity in the perturbative limit is the area for cylinders rather than the volume for spheres. It follows that ϕ is proportional to the two areas R_1^2 and R_2^2 , and inversely proportional to the fourth power of distance.

V. NON-UNIVERSAL CONTRIBUTIONS WITH DIELECTRIC MATTER IN SALTED WATER

The universal Casimir interaction was calculated in [50] for two dielectric cylinders in salted water, but the non universal contributions have never been analyzed in this geometry. In order to fill this gap, we need a robust model for the dielectric response of matter, as non universal contributions depend on this response. In the absence of an exact solution, we have also to produce a reasonably accurate estimate for the interaction between two cylinders. These requirements are tackled in the present section.

For describing dielectric properties of organic matter, we follow [62, 63] by considering tetradecane as a proxy for these properties. Its dielectric function is given by a Lorentz model, with parameters to be found in [64]. In addition, we model salted water as in [46, 51], with the contribution from the ions depending on their concentration. As we mentioned above, this contribution is critical for the universal contribution at the zero frequency, but it plays a negligible role at nonzero Matsubara frequencies, which are too large (at room temperature) to “feel” the effect of ionic conduction (when compared to electrons, ions have a much larger mass and their number per unit volume is much smaller). The tetradecane function is represented in Fig. 6 versus imaginary frequency $\omega = i\xi$ (i.e., after a Wick rotation, as is common for studies of the Casimir effect [29]), alongside the pure water function (i.e., disregarding the ionic contribution) taken from the model in [65]. The vertical dashed line on the figure shows the position of the first nonzero Matsubara frequency ξ_1 at room temperature. The figure indicates a nearly perfect index matching of biological matter and water at this frequency, which is at the root of the smallness of the non universal contributions to the Casimir interaction. Although the contribution of ions is negligible at this frequency, the index contrast grows sharply for lower frequencies, in particular as the effective response diverges for salted water. This Drude-like divergence caused by the dissolved ions is the reason why the universal contribution ends up not depending on the details of the properties of the material immersed in salted water.

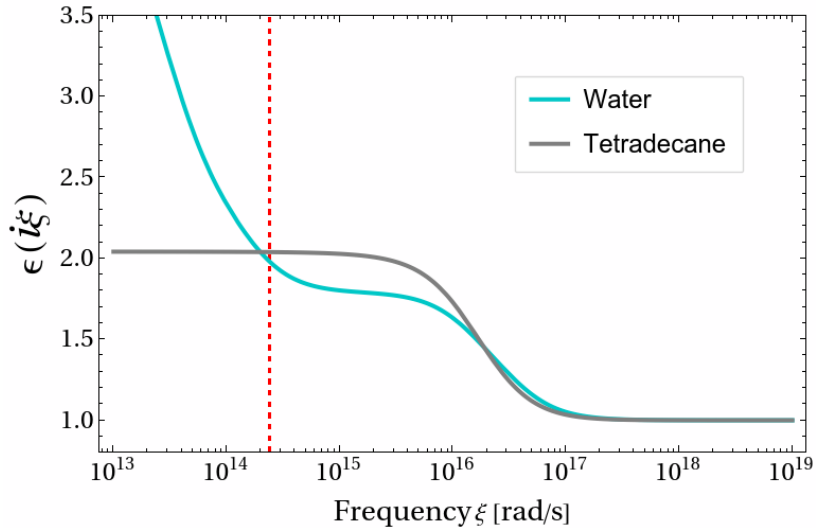


FIG. 6. Dielectric functions of water (blue) and tetradecane (gray) versus imaginary frequency ξ . The vertical dashed (red) line represents the first nonzero Matsubara frequency $\xi_1 = 2\pi k_B T / \hbar$ at ambient temperature, where the dielectric functions of water and tetradecane are nearly identical.

In order to get reliable estimations for the non universal contributions to interaction between cylinders, we use the fact that these contributions are expected to be small due to the index-matching at most non null Matsubara frequencies and, therefore, that they should be approximately represented by a pairwise summation technique [66]. We stress that such an approximation cannot give an accurate description of the universal contribution as perturbation theory is not at all adapted to this case. Guided by the pairwise summation, we shall take an educated guess and assume that the order of magnitude of the ratio between universal and non universal contributions arising from two cylinders of radii R can be roughly estimated from the same calculation in a setup of two slabs of thickness $w \equiv 2R$ separated by a gap d of salted water.

Rewriting expression (4) for slabs, we get

$$\mathcal{F}_{\text{Cas}}^{\text{slab}} = \mathcal{F}_0^{\text{slab}} + \sum_{n=1}^{\infty} \mathcal{F}_n^{\text{slab}}. \quad (16)$$

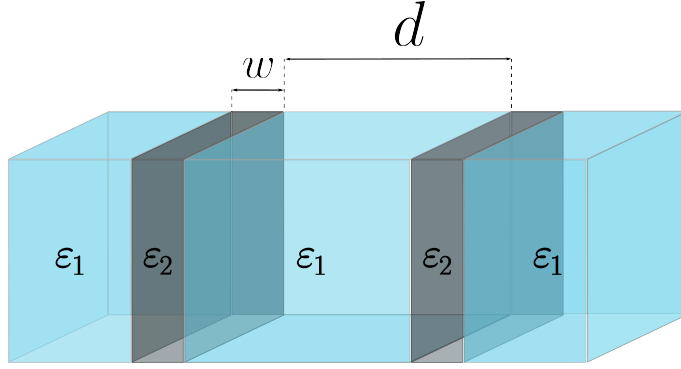


FIG. 7. Sketch view of the two-slabs configurations, with d the distance between the two parallel interfaces and w the width of the slabs (ε_1 and ε_2 defined as for Fig.1).

where the nonzero Matsubara terms are given by

$$\mathcal{F}_n^{\text{slab}} = A k_B T \sum_{\sigma} \int \frac{d^2 k}{(2\pi)^2} \ln \left(1 - \tilde{r}^{(\sigma)}(i\xi_n)^2 e^{-2\kappa_1 d} \right) , \quad n \neq 0 \quad (17)$$

with σ standing for either TE or TM polarization of a given electromagnetic mode. The reflection coefficients of a slab are given by [67]

$$\tilde{r}^{(\sigma)}(i\xi_n) = \frac{r^{(\sigma)}(i\xi_n)(1 - \exp(-2\kappa_2 w))}{1 - r^{(\sigma)}(i\xi_n)^2 \exp(-2\kappa_2 w)} , \quad \kappa_i = \sqrt{\epsilon_i(i\xi_n) \xi_n^2/c^2 + k^2} . \quad (18)$$

where $r^{(\sigma)}(i\xi_n)$ are the Fresnel coefficients for a plane wave going from the electrolyte to the slab

$$r^{(\text{TE})}(i\xi_n) = \frac{\kappa_1 - \kappa_2}{\kappa_1 + \kappa_2} , \quad r^{(\text{TM})}(i\xi_n) = \frac{\varepsilon_2 \kappa_1 - \varepsilon_1 \kappa_2}{\varepsilon_2 \kappa_1 + \varepsilon_1 \kappa_2} . \quad (19)$$

The zero-frequency Matsubara term $\mathcal{F}_0^{\text{slab}}$ for the slabs is analogous to expression (5). Given that we are interested in distances d largely beyond the Debye length, the longitudinal part is negligible

$$\mathcal{F}_0^{\text{slab}} \simeq \mathcal{F}_{\text{univ}}^{\text{slab}} . \quad (20)$$

As shown in the Appendix of [51], the universal contribution for two slabs is the same as in the case of two half-spaces discussed in §II: $\mathcal{F}_{\text{univ}}^{\text{slab}} = \mathcal{F}_{\text{univ}}^{\text{bulk}}$.

The variations of the universal contribution for the binding energy $|\mathcal{F}_{\text{univ}}^{\text{slab}}|$ and the non-universal part $|\sum_{n \geq 1} \mathcal{F}_n^{\text{slab}}|$ versus distance d are depicted separately in Fig. 8, for identical slabs of thickness $w = 6$ nm (this number is motivated by discussions in §VI). The non-universal contributions have been calculated with the dielectric model for tetradecane represented in Fig. 6. Figure 8 clearly shows that the non-universal contributions are much smaller than the universal one, which is a consequence of the index-matching at nonzero Matsubara frequencies between water and tetradecane. We have checked that the ratio between the two contributions is always above a factor 100.

VI. IMPLICATIONS AT THE CELL SCALE

We now use the results presented above to show how the universal Casimir interaction may play an important role in biomechanics at the cell scale. The question was thoroughly discussed in [50] where many references can be found. Here we only recall a few critical points.

Actin filaments play critical roles in the mechanical functions of the cytoskeleton as well as in many intracellular processes, by actively generating forces with the help of motor proteins [68–70]. They form bundles, with filaments cross-linked by specific proteins into parallel arrays. It has been shown that bundles of parallel filaments may form *in vitro* in the absence of cross-linkers [71, 72]. Other examples of self-assembled filaments are discussed in [50], which play key roles in or beyond the cytoskeleton. The universal Casimir interaction considered above is relevant

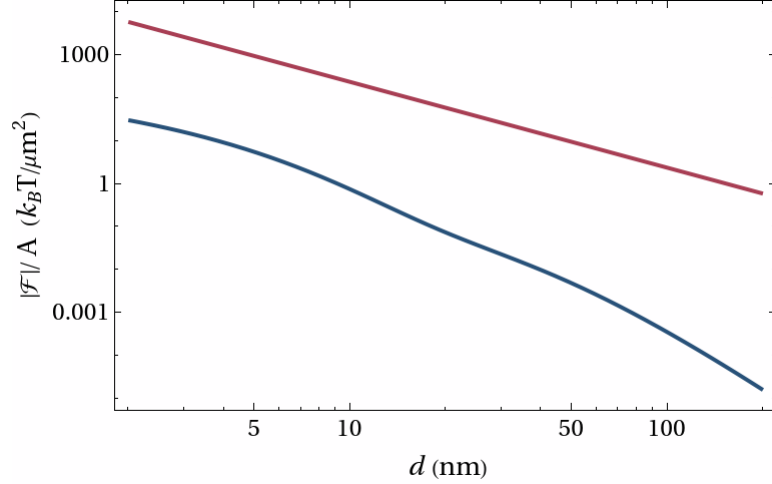


FIG. 8. Universal (red higher line) and non-universal (blue lower line) contributions to the Casimir binding energy, for two slabs of tetradecone of thickness $w = 6$ nm separated by a salted water gap d . The binding energy $|\mathcal{F}|$ per unit area are represented in units of thermal energy $k_B T$ per μm^2 .

at the observed dimensions for bundles of actin filaments, so that they should have important implications in the self-assembly and cohesion of bundles of filaments at the cell scale.

Estimation of the interaction for the relevant case of parallel actin filaments is done by modeling filaments as cylinders and using the physical dimensions known for parallel actin filaments [73], each having a radius $R \simeq 3$ nm and a length $L \simeq 15 \mu\text{m}$, which form bundles with typical distance of closest approach $d \simeq 6$ nm between filaments (geometry sketched as an inset in Fig. 9 with filaments shown in blue and cross-linkers in red). These numbers lead to a large value for the ratio $L/d \simeq 2500$, which is a key reason for which the correspondent Casimir interaction is so significant. The binding energy $|\mathcal{F}|$ expressed in units of $k_B T$ is shown versus the separation distance d in Fig. 9. The relevant distance $d \simeq 6$ nm is emphasized as the red point on the plot, where the binding energy is of the order of $5 k_B T$. In the gray-shaded zone, $|\mathcal{F}|$ is dominated by the Brownian motion energy $k_B T$.

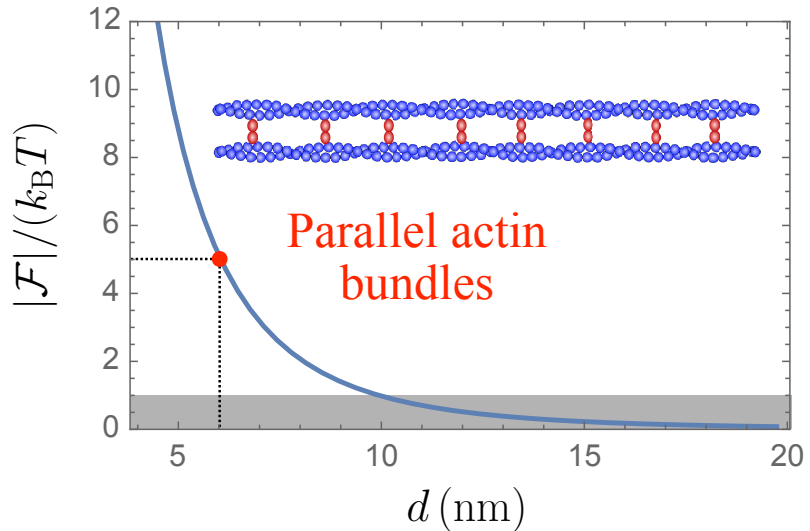


FIG. 9. Casimir binding free energy between actin filaments having each a radius 3 nm and a length 15 μm . The binding free energy $|\mathcal{F}|$ is drawn versus the distance d (nm) between two parallel actin filaments and measured in units of $k_B T$. In the gray-shaded zone $|\mathcal{F}|$ is dominated by the thermal energy $k_B T$. Energies above this zone are relevant for biomechanics in the cell, and they include the physiological distance (6 nm) indicated by the red marker. Inset: schematic of two actin filaments (blue) in a two-filaments bundle, with cross-linkers shown in red. Adapted from Spreng et al. [50] under the terms of the Creative Commons Attribution 4.0 International license.

We stress at this point that such a magnitude had to be expected for a physical interaction having relevance for biomechanics at the cell scale. The interaction has to be larger than $k_B T$ in order to dominate Brownian agitation while it should not be too large to be compatible with a mechanical activity provided by molecular motors. This was underlined by Moysés Nussenzveig in his remarkable paper [53] commenting on the links between physics and biology, and discussing in particular the pioneering works of Bohr [74] and Schrödinger [75].

We also emphasize that this magnitude has been obtained without any *ad hoc* fine-tuning of the parameters. The energy constants are given by the theory of the universal Casimir interaction reviewed in this paper, and they do not depend on any specific detail for the biological matter involved. Hence the binding energy depends only on geometrical parameters known for bundles of actin filaments [73]. Note also that the numbers presented for actin (red marker shown on Fig. 9) correspond to $x = 4$ in Fig. 5b, where the PFA expression largely overestimates the correct value of ϕ . This implies that the calculation presented in [50] for cylinders was mandatory for obtaining a reliable estimation for bundles of actin filaments.

Another important point is clear after the discussions in the present paper. We have given an estimation of the non universal Casimir interaction in §V, and shown that it is more than a hundred times smaller than the universal one. It is thus clear that the non universal interaction is not only much smaller than the universal one, but also much too small to have any relevance in a medium dominated by Brownian agitation. It is only the presence of the universal contribution which makes the Casimir binding energy important for biomechanics at the cell scale.

As a concluding remark, we want to stress that physics is extremely complex at the cell scale, with a large number of different processes involved in the mechanics and functionalities of the cell. Detailed discussions of this very important fact are presented in the concluding part of [50]. Our modest aim in this review has only been to show that the universal Casimir interaction due to transverse electromagnetic fluctuations has to be considered as a significant contribution to this rich physics as it produces an attractive interaction between biological filaments in the cell with a typical energy of a few Brownian thermal scales $k_B T$.

ACKNOWLEDGMENTS

This paper is dedicated to the memory of our dear and esteemed colleague, H. Moysés Nussenzveig, to whom we are indebted for many inspiring discussions.

The authors warmly thank the colleagues who have participated in the development of this project over the years, in particular D.S. Ether, L.B. Pires, S. Umrath, D. Martinez, Y. Ayala, B. Pontes, G.R.S. Araújo, S. Frases, G.-L. Ingold, N.B. Viana, R.O. Nunes, A.B. Moraes, A. Canaguier-Durand, R. Guérout, B. Spreng, M.J.B. Moura, R.S. Decca, R.S. Dutra, M. Borges, T. Schoger, H. Berthoumieux, A.-F. Bitbol.

This work was supported by CAPES-COFECUB collaboration project n° Ph1030/24, Conselho Nacional de Desenvolvimento Científico e Tecnológico (CNPq-Brazil), Instituto Nacional de Ciência e Tecnologia de Fluidos Complexos (INCT-FCx), and the Research Foundations of the States of Rio de Janeiro (FAPERJ) and São Paulo (FAPESP).

L.I. was supported by the project No. 2022/47/P/ST3/01236 co-funded by the National Science Centre and the European Union's Horizon 2020 research and innovation programme under the Marie Skłodowska-Curie grant agreement No. 945339. Institutional and infrastructural support for the ENSEMBLE3 Centre of Excellence was provided through the ENSEMBLE3 project (MAB/2020/14) delivered within the Foundation for Polish Science International Research Agenda Programme and co-financed by the European Regional Development Fund and the Horizon 2020 Teaming for Excellence initiative (Grant Agreement No. 857543), as well as the Ministry of Education and Science initiative "Support for Centres of Excellence in Poland under Horizon 2020" (MEiN/2023/DIR/3797).

[1] M. Planck, Theory of the energy distribution law in the normal spectrum (in german), *Verh. Deutsch. Phys. Ges.* **2**, 237 (1900).

[2] M. Planck, On a new radiation hypothesis (in german), *Verh. Deutsch. Phys. Ges.* **13**, 139 (1911).

[3] M. J. Klein, Thermodynamics and quanta in planck's work, *Physics Today* **19**, 23 (1966).

[4] O. Darrigol, Statistics and combinatorics in early quantum theory, *Historical studies in the physical and biological sciences* **19**, 17 (1988).

[5] A. Einstein and O. Stern, Some arguments for the assumption of molecular agitation at absolute zero (in german), *Annalen der Physik* **345**, 551 (1913).

[6] P. Milonni and M.-L. Shih, Zero-point energy in early quantum theory, *American Journal of Physics* **59**, 684 (1991).

[7] W. Nernst, On an attempt to return from quantum-theoretical considerations to the assumption of continuous energy changes (in german), *Verhandlungen der Deutschen Physikalischen Gesellschaft* **4** (1916).

[8] H. Kragh, Preludes to dark energy: zero-point energy and vacuum speculations, *Archive for history of exact sciences* **66**, 199 (2012).

[9] W. Heisenberg, On the quantum-theoretical reinterpretation of kinematical and mechanical relationships (in german), *Z. Physik* **33**, 879 (1925).

[10] M. Born and P. Jordan, On quantum mechanics (in german), *Zeitschrift für Physik* **34**, 858 (1925).

[11] P. A. M. Dirac, The fundamental equations of quantum mechanics, *Proceedings of the Royal Society of London. Series A, Containing Papers of a Mathematical and Physical Character* **109**, 642 (1925).

[12] M. Born, W. Heisenberg, and P. Jordan, On quantum mechanics ii (in german), *Zeitschrift für Physik* **35**, 557 (1926).

[13] B. L. Van Der Waerden, *Sources of quantum mechanics* (North Holland, 1967) reprinted by Dover 2007.

[14] W. Heisenberg, The actual content of quantum theoretical kinematics and mechanics (in german), *Zeitschrift für Physik* **43**, 172 (1927).

[15] O. Darrigol, *From c-numbers to q-numbers: The classical analogy in the history of quantum theory*, Vol. 8 (Univ of California Press, 1992).

[16] W. A. Fedak and J. J. Prentis, The 1925 born and jordan paper “on quantum mechanics”, *American journal of physics* **77**, 128 (2009).

[17] A. Duncan and M. Janssen, Heisenberg’s umdeutung paper, in *Constructing Quantum Mechanics Volume Two: The Arch, 1923-1927* (Oxford University Press, 2023).

[18] P. A. M. Dirac, The quantum theory of the emission and absorption of radiation, *Proceedings of the Royal Society of London. Series A* **114**, 243 (1927).

[19] A. Einstein, Quantum theory of radiation (in german), *Phys. Zeitschrift* **18**, 121 (1917).

[20] E. A. Power, Zero-point energy and the lamb shift, *American Journal of Physics* **34**, 516 (1966).

[21] J. Dupont-Roc, C. Fabre, and C. Cohen-Tannoudji, Physical interpretations for radiative corrections in the non-relativistic limit, *Journal of Physics B* **11**, 563 (1978).

[22] C. Itzykson and J.-B. Zuber, *Quantum field theory* (Mc Graw Hill, 1985).

[23] C. Cohen-Tannoudji, G. Grynberg, and J. Dupont-Roe, *Atom-photon interactions* (New York, NY (United States); John Wiley and Sons Inc., 1992).

[24] P. W. Milonni, *The quantum vacuum: an introduction to quantum electrodynamics* (Academic press, 2013).

[25] H. B. G. Casimir, On the attraction between two perfectly conducting plates, *Proc. Kon. Ned. Akad. Wetenschappen* **51**, 79 (1948).

[26] K. A. Milton, *The Casimir effect: physical manifestations of zero-point energy* (World Scientific, 2001).

[27] E. A. Power, Casimir-polder potential from first principles, *European Journal of Physics* **22**, 453 (2001).

[28] V. A. Parsegian, *Van der Waals forces: a handbook for biologists, chemists, engineers, and physicists* (Cambridge university press, 2005).

[29] S. Reynaud and A. Lambrecht, Casimir forces and vacuum energy, in *Quantum Optics and Nanophotonics*, Lecture Notes of the Les Houches Summer School 101 (Oxford University Press, 2017) pp. 407–455.

[30] D. Dalvit, P. Milonni, D. Roberts, and F. Da Rosa, *Casimir physics*, Vol. 834 (Springer, 2011).

[31] G. Palasantzas, D. A. R. Dalvit, R. Decca, V. B. Svetovoy, and A. Lambrecht, Casimir physics, *Journal of Physics: Condensed Matter* **27**, 210301 (2015).

[32] L. M. Woods, D. A. R. Dalvit, A. Tkatchenko, P. Rodriguez-Lopez, A. W. Rodriguez, and R. Podgornik, Materials perspective on casimir and van der Waals interactions, *Reviews of Modern Physics* **88**, 045003 (2016).

[33] A. Stange, D. K. Campbell, and D. J. Bishop, Science and technology of the casimir effect, *Physics Today* **74**, 42 (2021).

[34] K. A. Milton, *State of the Quantum Vacuum, The Casimir Physics in the 2020’s* (World Scientific, 2022).

[35] C. Shelden, B. Spreng, and J. Munday, Opportunities and challenges involving repulsive Casimir forces in nanotechnology, *Applied Physics Reviews* **11**, 10.1063/5.0218274 (2024).

[36] J. Mehra, Temperature correction to the casimir effect, *Physica* **37**, 145 (1967).

[37] L. S. Brown and G. J. Maclay, Vacuum stress between conducting plates: an image solution, *Physical Review* **184**, 1272 (1969).

[38] J. Schwinger, L. L. DeRaad Jr, and K. A. Milton, Casimir effect in dielectrics, *Annals of Physics* **115**, 1 (1978).

[39] T. Matsubara, A new approach to quantum-statistical mechanics, *Progress of theoretical physics* **14**, 351 (1955).

[40] A. Lambrecht, P. A. Maia Neto, and S. Reynaud, The casimir effect within scattering theory, *New Journal of Physics* **8**, 243 (2006).

[41] J. Feinberg, A. Mann, and M. Revzen, Casimir effect: The classical limit, *Annals of Physics* **288**, 103 (2001).

[42] A. Canaguier-Durand, G.-L. Ingold, M.-T. Jaekel, A. Lambrecht, P. A. Maia Neto, and S. Reynaud, Classical casimir interaction in the plane-sphere geometry, *Phys. Rev. A* **85**, 052501 (2012).

[43] R. S. Decca, V. Aksyuk, and D. López, Casimir Force in Micro and Nano Electro Mechanical Systems, in *Casimir Physics*, Lecture Notes in Physics, Vol. 834 (Springer, 2011) pp. 287–309.

[44] G. Bimonte, B. Spreng, P. A. Maia Neto, G.-L. Ingold, G. L. Klimchitskaya, V. M. Mostepanenko, and R. S. Decca, Measurement of the casimir force between 0.2 and 8 μm : Experimental procedures and comparison with theory, *Universe* **7**, 93 (2021).

[45] D. S. Ether, L. B. Pires, S. Umrath, D. Martinez, Y. Ayala, B. Pontes, G. R. de S. Araújo, S. Frases, G.-L. Ingold, F. S. S. Rosa, N. B. Viana, H. M. Nussenzveig, and P. A. M. Neto, Probing the casimir force with optical tweezers, *Europhysics Letters* **112**, 44001 (2015).

[46] P. A. Maia Neto, F. S. S. Rosa, L. B. Pires, A. B. Moraes, A. Canaguier-Durand, R. Guérout, A. Lambrecht, and S. Reynaud, Scattering theory of the screened casimir interaction in electrolytes, *The European Physical Journal D* **73**,

178 (2019).

[47] L. B. Pires, D. S. Ether, B. Spreng, G. R. S. Araújo, R. S. Decca, R. S. Dutra, M. Borges, F. S. S. Rosa, G.-L. Ingold, M. J. B. Moura, S. Frases, B. Pontes, H. M. Nussenzveig, S. Reynaud, N. B. Viana, and P. A. Maia Neto, Probing the screening of the casimir interaction with optical tweezers, *Phys. Rev. Res.* **3**, 033037 (2021).

[48] T. Schoger, B. Spreng, G.-L. Ingold, P. A. Maia Neto, and S. Reynaud, Universal Casimir interaction between two dielectric spheres in salted water, *Physical Review Letters* **128**, 10.1103/PhysRevLett.128.230602 (2022).

[49] T. Schoger, B. Spreng, G.-L. Ingold, A. Lambrecht, P. A. Maia Neto, and S. Reynaud, Universal Casimir interactions in the sphere-sphere geometry, *International Journal of Modern Physics A* **37**, 10.1142/S0217751X22410056 (2022).

[50] B. Spreng, H. Berthoumieux, A. Lambrecht, A.-F. Bitbol, P. A. Maia Neto, and S. Reynaud, Universal casimir attraction between filaments at the cell scale, *New Journal of Physics* **26**, 013009 (2024).

[51] L. Inácio, F. S. Rosa, S. Reynaud, and P. A. Maia Neto, Casimir repulsion turned into attraction by the nonlocal response of salted water, *Phys. Rev. A* **111**, 012816 (2025).

[52] A. Ashkin, *Optical Trapping and Manipulation of Neutral Particles Using Lasers: A Reprint Volume with Commentaries* (WORLD SCIENTIFIC PUB CO INC, 2007).

[53] H. M. Nussenzveig, Bohr's 'light and life' revisited, *Physica Scripta* **90**, 118001 (2015).

[54] C. J. Bustamante, Y. R. Chemla, S. Liu, and M. D. Wang, Optical tweezers in single-molecule biophysics, *Nature Reviews Methods Primers* **1**, 25 (2021).

[55] N. B. Viana, M. S. Rocha, O. N. Mesquita, A. Mazolli, P. A. Maia Neto, and H. M. Nussenzveig, Towards absolute calibration of optical tweezers, *Phys. Rev. E* **75**, 021914 (2007).

[56] R. S. Dutra, N. B. Viana, P. A. Maia Neto, and H. M. Nussenzveig, Absolute calibration of forces in optical tweezers, *Physical Review A* **90**, 013825 (2014).

[57] M. Sarshar, W. Wong, and B. Anvari, Comparative study of methods to calibrate the stiffness of a single-beam gradient-force optical tweezers over various laser trapping powers, *Journal of Biomedical Optics* **19**, 115001 (2014).

[58] B. Spreng, P. A. Maia Neto, and G.-L. Ingold, Plane-wave approach to the exact van der Waals interaction between colloid particles, *The Journal of Chemical Physics* **153**, 024115 (2020).

[59] V. A. Parsegian, *Van der Waals forces: a handbook for biologists, chemists, engineers, and physicists* (Cambridge university press, 2005).

[60] R. O. Nunes, B. Spreng, R. de Melo e Souza, G.-L. Ingold, P. A. Maia Neto, and F. S. S. Rosa, The Casimir interaction between spheres immersed in electrolytes, *Universe* **7**, 156 (2021).

[61] B. Spreng, M. Hartmann, V. Henning, P. A. Maia Neto, and G.-L. Ingold, Proximity force approximation and specular reflection: Application of the wkb limit of mie scattering to the casimir effect, *Phys. Rev. A* **97**, 062504 (2018).

[62] V. Parsegian and B. Ninham, Temperature-dependent van der Waals forces, *Biophysical Journal* **10**, 664 (1970).

[63] V. Parsegian and B. Ninham, Toward the correct calculation of van der Waals interactions between lyophobic colloids in an aqueous medium, *Journal of Colloid and Interface Science* **37**, 332 (1971).

[64] V. Parsegian and G. H. Weiss, Spectroscopic parameters for computation of van der Waals forces, *Journal of Colloid and Interface Science* **81**, 285 (1981).

[65] P. J. van Zwol and G. Palasantzas, Repulsive casimir forces between solid materials with high-refractive-index intervening liquids, *Phys. Rev. A* **81**, 062502 (2010).

[66] A.-F. Bitbol, A. Canaguier-Durand, A. Lambrecht, and S. Reynaud, Pairwise summation approximation for casimir potentials and its limitations, *Phys. Rev. B* **87**, 10.1103/PhysRevB.87.045413 (2013).

[67] I. Pirozhenko and A. Lambrecht, Influence of slab thickness on the casimir force, *Phys. Rev. A* **77**, 013811 (2008).

[68] G. Salbreux, G. Charras, and E. Paluch, Actin cortex mechanics and cellular morphogenesis, *Trends Cell Biol* **22**, 536 (2012).

[69] M. Murrell, P. W. Oakes, M. Lenz, and M. L. Gardel, Forcing cells into shape: the mechanics of actomyosin contractility, *Nat Rev Mol Cell Biol* **16**, 486 (2015).

[70] F. Burla, Y. Mulla, B. E. Vos, A. Aufderhorst-Roberts, and G. H. Koenderink, From mechanical resilience to active material properties in biopolymer networks, *Nature Reviews Physics* **1**, 249 (2019).

[71] J. X. Tang and P. A. Janmey, The polyelectrolyte nature of F-actin and the mechanism of actin bundle formation, *J Biol Chem* **271**, 8556 (1996).

[72] S. Deshpande and T. Pfohl, Hierarchical self-assembly of actin in micro-confinements using microfluidics, *Biomicrofluidics* **6**, 34120 (2012).

[73] N. Volkmann, D. DeRosier, P. Matsudaira, and D. Hanein, An atomic model of actin filaments cross-linked by fimbrin and its implications for bundle assembly and function, *Journal of Cell Biology* **153**, 947 (2001).

[74] N. Bohr, Light and life, *Nature* **131**, 457 (1933).

[75] E. Schrödinger, *What is life? The physical aspect of the living cell* (Cambridge University Presss, 1944).